Optimized Pulse Patterns for Converters Connected to a Distorted Grid via LCL Filters

Shirin Rahmanpour
Faculty of Inf. Technol. and Commun. Sciences
Tampere University
Tampere, Finland
shirin.rahmanpour@tuni.fi

Petros Karamanakos
Faculty of Inf. Technol. and Commun. Sciences
Tampere University
Tampere, Finland
p.karamanakos@ieee.org

Tobias Geyer
Motion System Drives
ABB Switzerland Ltd
Turgi, Switzerland
t.geyer@ieee.org

Abstract—**This paper presents the computation of optimized pulse patterns (OPPs) for converters connected to the grid via LCL filters. The computed OPPs account for distortions in the grid, such as harmonics injected to the point of common coupling (PCC) by other converters. To this aim, the contribution of different harmonic sources is modeled and included in the OPP optimization problem. By augmenting the said optimization problem with explicit constraints on current and voltage harmonics at the PCC, the computed OPPs ensure that harmonic grid standards are fully met. The presented numerical results demonstrate the superior harmonic performance of the proposed OPPs in the presence of harmonic disturbances.**

Index Terms—**Grid-connected converters, grid standards, harmonic distortions, optimized pulse patterns (OPPs), pulse width modulation (PWM).**

I. Introduction

The output voltage and current of grid-connected converters have to be of high quality as they need to abide by harmonic grid codes, such as the IEEE 519 [1] and IEC 61000-2-4 [2] standards. To this aim, the converter is usually connected to the grid via an LCL filter such that harmonics above the filter resonance frequency are effectively attenuated.

Nevertheless, the modulation also affects the quality of the output, especially when the ratio of switching-to-fundamental frequency is relatively low or when the converter operates at switching frequencies close to the filter resonance frequency. Under such conditions, conventional pulse width modulation (PWM) methods, such as carrier-based PWM (CB-PWM) or space vector modulation (SVM), oftentimes fail to meet the desired harmonic performance [3]. For this reason, more sophisticated modulation methods are required, such as programmed PWM in the form of selective harmonic elimination/mitigation (SHE/SHM) or optimized pulse patterns (OPPs) [4], [5].

More specifically, SHE/SHM methods can be more effective than conventional PWM methods as they can be designed to eliminate/mitigate specific harmonics such that the harmonic grid standards can be met [6]–[9]. On the downside, many SHE/SHM methods struggle with eliminating/mitigating a high number of harmonics as solving the associated system of non-linear equations/inequalities becomes very challenging, if not impossible. On the other hand, OPPs tend to perform better as they are computed based on an optimization problem that minimizes the output current total demand distortion

(TDD), while tackling targeted harmonics. Nevertheless, both SHE/SHM-based pulse patterns and OPPs are commonly computed for first-order systems, i.e., a converter with an inductive load, meaning that they do not account for the LCL filter. Consequently, their harmonic performance is not the most favorable when higher-order systems are of concern, such as grid-connected converters with LCL filters.

To improve the performance of OPPs when applied to higher-order systems, the objective function, i.e., the current TDD, of the OPP optimization problem in [10] accounted for the LCL filter transfer function from the switching signal to the grid current. In doing so, the output current quality significantly improved. This work, however, did not ensure that the output current could comply with the grid standards. To address this, in a similar fashion to SHM techniques, [11] added constraints to the OPP problem such that the current harmonics would not violate their stringent limits dictated by the harmonic grid standards. To facilitate this, that work also relaxed artificial limitations, such as symmetry and switching properties, that are typically imposed on OPPs. As shown in [12], such relaxations increase the search space, thus enabling the reduction of the current TDD while meeting additional goals [13], [14].

Despite the improved performance of the tailored OPPs in [10] and [11], they are computed on the assumption of an ideal grid. Therefore, when, e.g., harmonics are injected into the point of common coupling (PCC) by other converters, the harmonic performance of OPPs is compromised. This problem was considered to some degree in [15], which proposed a SHM method aiming to meet current harmonic requirements while considering the contribution of both grid and converter voltage harmonics. Moreover, artificial neural networks were used in [16] for the real-time manipulation of patterns obtained by selective harmonic control (SHC) PWM such that grid disturbances were accounted for. It is noteworthy, however, that the methods in both [15] and [16] were developed for and applied to first-order systems.

Motivated by the above, this paper reformulates the OPP optimization problem for grid-connected converters with LCL filters such that both current and voltage harmonics comply with relevant grid standards in the presence of harmonic voltages—referred to as disturbances—generated by other con-
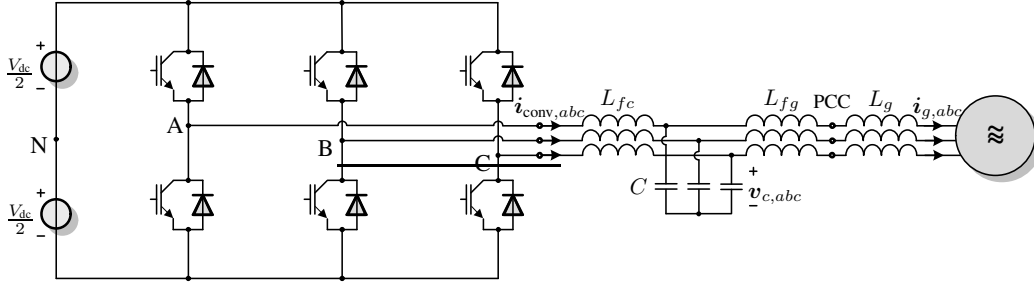
Fig. 1: Two-level converter connected to the grid via an LCL filter.

verters at the PCC. To this aim, the OPP optimization problem in [11] is modified to account not only for the switching function harmonics but also for the PCC disturbances. As demonstrated by the numerical results, the proposed harmonic-constrained OPPs exhibit significantly better performance compared with existing modulation methods when harmonic disturbances exist at the PCC.
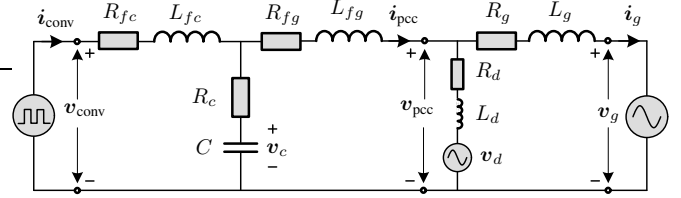
II. OPPs FOR GRID-CONNECTED CONVERTERS WITH LCL FILTERS

The OPPs are computed for a low-voltage (LV) power electronic system consisting of a two-level converter connected to the grid via an LCL filter, see Fig. 1. This section provides the system model used in the optimization problem. Subsequently, the computation of OPPs that meet grid standards in the presence of harmonic disturbances at the PCC is presented.
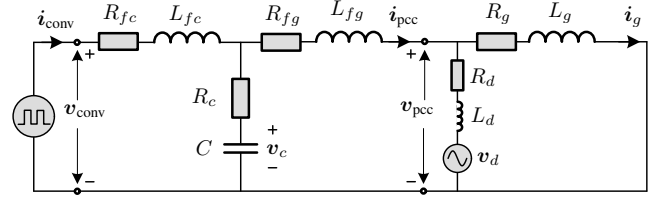
A. Modeling of the Grid-Connected Converter System

For the derivation of the differential equations that describe the dynamics of the system in question, the $\alpha\beta$-frame equivalent circuit in Fig. 2 is employed. Therein, Fig. 2(a) represents the equivalent circuit for both fundamental and harmonic components, while Fig. 2(b) is the harmonic model of the system, implying that the grid voltage is discarded as it does not have ripple. As this circuit is the basis for the harmonic analysis that follows, it is further divided into those in Figs. 2(c) and 2(d), depending on the source of PCC voltage and current harmonics. As can be seen, one source of harmonics is the converter of interest (Fig. 2(c)) and other source is other converters connected to the PCC (Fig. 2(d)). All other converters connected to the PCC are modeled by an equivalent voltage source $\boldsymbol{v}_d$, which has both fundamental and harmonic components. Moreover, it is assumed that each of the converters is connected to the PCC via a transformer, modeled with the (lumped) inductance L_d and its equivalent series resistance R_d. Note that the voltage at the terminals of the branch that models the other converters, i.e., $\boldsymbol{v}_{\mathrm{pcc},2}$, is considered as the disturbance to the system. To obtain the system model, the following procedure is adopted.
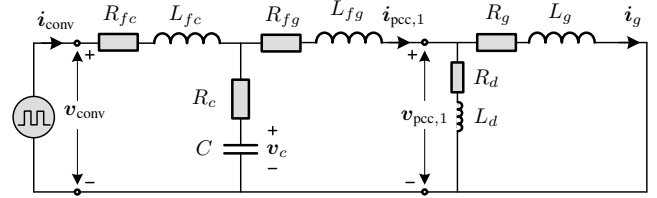
Step 1: To investigate the contribution of the converter of interest to the current and voltage harmonics at the PCC, $\boldsymbol{v}_d$ is considered as a short-circuit, see Fig. 2(c). This yields[1]

---

[1]For notational simplicity, the $\alpha\beta$ subscript is dropped from variables in the said frame, whereas variables in the abc-frame have their subscript stated.
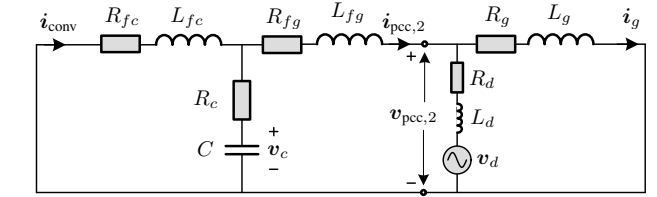

(a) Fundamental and harmonic model ($n > 0$)

(b) Harmonic model ($n > 1$)

(c) Harmonic model with the contribution of the converter

(d) Harmonic model with the contribution of the disturbances

Fig. 2: Equivalent circuit of the converter system in the $\alpha\beta$-frame.

$$L_{fc}\frac{\mathrm{d}\boldsymbol{i}_{\mathrm{conv}}(t)}{\mathrm{d}t} = -R_1\boldsymbol{i}_{\mathrm{conv}}(t) + R_c\,\boldsymbol{i}_{\mathrm{pcc},1}(t) - \boldsymbol{v}_c(t) + \boldsymbol{v}_{\mathrm{conv}}(t) \tag{1a}$$

$$L_1\frac{\mathrm{d}\boldsymbol{i}_{\mathrm{pcc},1}(t)}{\mathrm{d}t} = R_c\,\boldsymbol{i}_{\mathrm{conv}}(t) - R_2\,\boldsymbol{i}_{\mathrm{pcc},1}(t) + \boldsymbol{v}_c(t) \tag{1b}$$

$$\frac{\mathrm{d}\boldsymbol{v}_c(t)}{\mathrm{d}t} = \frac{1}{C}\,\boldsymbol{i}_{\mathrm{conv}}(t) - \frac{1}{C}\,\boldsymbol{i}_{\mathrm{pcc},1}(t)\,, \tag{1c}$$

where $\boldsymbol{i}_{\mathrm{conv}}$ is the converter current, $\boldsymbol{i}_{\mathrm{pcc},1}$ the PCC current due to the converter, and $\boldsymbol{v}_c$ the filter capacitor voltage. Moreover, the converter output voltage is

$$\boldsymbol{v}_{\mathrm{conv}}(t) = \frac{V_{\mathrm{dc}}}{2}\boldsymbol{K}\boldsymbol{u}_{abc}(t)\,,$$

with V_{dc} being the dc-link voltage, $\boldsymbol{u}_{abc} = [u_a \ u_b \ u_c]^T \in \{-1,1\}^3$ the three-phase switch position, and $\boldsymbol{K}$ a transformation matrix that maps quantities in the three-phase (abc) plane into quantities in the stationary, orthogonal ($\alpha\beta$) plane. Furthermore, the resistance $R_1 = R_{fc} + R_c$ in (1) comprises the series resistances of the converter-side filter inductance L_{fc} and capacitance C, respectively. Moreover, $L_1 = L_{fg} + L_{eq}$ combines the grid-side filter inductance L_{fg} and the equivalent inductance L_{eq} obtained from the parallel branches on the right-hand side of the circuit in Fig. 2(c), i.e., the branches consisting of the impedance of the grid and that of the other converters connected to the PCC. In addition, the series resistance of the grid-side filter inductance R_{fg}, and the equivalent resistance of the parallel branches R_{eq} are considered in $R_2 = R_c + R_{fg} + R_{eq}$.

Based on the above, the dynamics in Fig. 2(c) can be described with the state vector $\boldsymbol{x}_1 = [\boldsymbol{i}_{conv}^T \ \boldsymbol{i}_{pcc,1}^T \ \boldsymbol{v}_c^T]^T \in \mathbb{R}^6$, while the three-phase switch position $\boldsymbol{u}_{abc}$ is the system input, and the PCC current and voltage are the system outputs, i.e., $\boldsymbol{y}_1 = \boldsymbol{i}_{pcc,1} \in \mathbb{R}^2$ and $\boldsymbol{y}_1' = \boldsymbol{v}_{pcc,1} \in \mathbb{R}^2$, respectively. Hence, the state-space model of the system in Fig. 2(c) is

$$
\begin{aligned}
\frac{d\boldsymbol{x}_1(t)}{dt} &= \boldsymbol{A}_1 \boldsymbol{x}_1(t) + \boldsymbol{B}_1 \boldsymbol{u}_{abc}(t) \\
\boldsymbol{y}_1(t) &= \boldsymbol{C}_1 \boldsymbol{x}_1(t) \\
\boldsymbol{y}_1'(t) &= \boldsymbol{C}_1' \boldsymbol{x}_1(t) \,,
\end{aligned}
\tag{2}
$$

where the state-space matrices are obtained from (1). With (2), the transfer matrices from the system input to the outputs $\boldsymbol{i}_{pcc,1}$ and $\boldsymbol{v}_{pcc,1}$ can be derived, i.e.,

$$
\begin{aligned}
\boldsymbol{H}_1(s) &= \mathcal{L}\{\boldsymbol{i}_{pcc,1}\}(s)/\mathcal{L}\{\boldsymbol{u}_{abc}\}(s) \,, \\
\boldsymbol{H}_2(s) &= \mathcal{L}\{\boldsymbol{v}_{pcc,1}\}(s)/\mathcal{L}\{\boldsymbol{u}_{abc}\}(s) \,.
\end{aligned}
$$

These matrices help mapping the effect of the applied pulse patterns on the PCC current and voltage harmonics, as shown later.

Step 2: To investigate the impact of the system disturbances, e.g., of the other converters connected to the PCC, on the current and voltage harmonics at the PCC, the converter under study appears as a short-circuit. As a result, the circuit in Fig. 2(d) is described by

$$
L_{fc} \frac{d\boldsymbol{i}_{conv}(t)}{dt} = -R_1 \boldsymbol{i}_{conv}(t) + R_c \boldsymbol{i}_{pcc,2}(t) - \boldsymbol{v}_c(t) \tag{3a}
$$

$$
L_{fg} \frac{d\boldsymbol{i}_{pcc,2}(t)}{dt} = R_c \boldsymbol{i}_{conv}(t) - R_3 \boldsymbol{i}_{pcc,2}(t) + \boldsymbol{v}_c(t) - \boldsymbol{v}_{pcc,2}(t) \tag{3b}
$$

$$
\frac{d\boldsymbol{v}_c(t)}{dt} = \frac{1}{C} \boldsymbol{i}_{conv}(t) - \frac{1}{C} \boldsymbol{i}_{pcc,2}(t) \tag{3c}
$$

$$
L_g \frac{d\boldsymbol{i}_g(t)}{dt} = -R_g \boldsymbol{i}_g(t) + \boldsymbol{v}_{pcc,2}(t) \,, \tag{3d}
$$

where $\boldsymbol{i}_{pcc,2}$ is the PCC current due to the harmonic disturbances, while the corresponding PCC voltage is $\boldsymbol{v}_{pcc,2}(t) = \boldsymbol{K}\boldsymbol{v}_{pcc,2,abc}(t)$. Moreover, $\boldsymbol{i}_g$ is the grid current, and $R_3 = R_c + R_{fg}$.

For the harmonic model in Fig. 2(d), the state vector is

chosen as $\boldsymbol{x}_2 = [\boldsymbol{i}_{conv}^T \ \boldsymbol{i}_{pcc,2}^T \ \boldsymbol{v}_c^T \ \boldsymbol{i}_g^T]^T \in \mathbb{R}^8$, while the PCC current and voltage are considered as the system outputs, i.e., $\boldsymbol{y}_2 = \boldsymbol{i}_{pcc,2} \in \mathbb{R}^2$ and $\boldsymbol{y}_2' = \boldsymbol{v}_{pcc,2} \in \mathbb{R}^2$, respectively. Given (3), and with the three-phase PCC voltage $\boldsymbol{v}_{pcc,2,abc}$ as the disturbance, the state-space model of the system is

$$
\begin{aligned}
\frac{d\boldsymbol{x}_2(t)}{dt} &= \boldsymbol{A}_2 \boldsymbol{x}_2(t) + \boldsymbol{B}_2 \boldsymbol{v}_{pcc,2,abc}(t) \\
\boldsymbol{y}_2(t) &= \boldsymbol{C}_2 \boldsymbol{x}_2(t) \\
\boldsymbol{y}_2'(t) &= \boldsymbol{C}_2' \boldsymbol{x}_2(t) + \boldsymbol{D}' \boldsymbol{v}_{pcc,2,abc}(t) \,.
\end{aligned}
\tag{4}
$$

Note that, with (4), the transfer matrices from the disturbance $\boldsymbol{v}_{pcc,2,abc}$ to the system outputs can be obtained, i.e.,

$$
\begin{aligned}
\boldsymbol{H}_3(s) &= \mathcal{L}\{\boldsymbol{i}_{pcc,2}\}(s)/\mathcal{L}\{\boldsymbol{v}_{pcc,2,abc}\}(s) \,, \\
\boldsymbol{H}_4(s) &= \mathcal{L}\{\boldsymbol{v}_{pcc,2}\}(s)/\mathcal{L}\{\boldsymbol{v}_{pcc,2,abc}\}(s) \,.
\end{aligned}
$$

As previously, these transfer matrices are used for mapping the effect of harmonic disturbances on the PCC current and voltage harmonics.

Step 3: According to the principle of superposition, the current and voltage at the PCC are computed by combining the contributions from the converter voltage and the disturbance. In doing so, the PCC current in the frequency domain becomes

$$
\begin{aligned}
\boldsymbol{i}_{pcc}(s) &= \boldsymbol{i}_{pcc,1}(s) + \boldsymbol{i}_{pcc,2}(s) \\
&= \boldsymbol{H}_1(s) \boldsymbol{u}_{abc}(s) + \boldsymbol{H}_3(s) \boldsymbol{v}_{pcc,2,abc}(s) \,,
\end{aligned}
\tag{5}
$$

which in the abc-frame is

$$
\begin{aligned}
\boldsymbol{i}_{pcc,abc}(s) &= \boldsymbol{K}^{-1} \boldsymbol{i}_{pcc}(s) \\
&= \boldsymbol{M}(s) \boldsymbol{u}_{abc}(s) + \boldsymbol{N}(s) \boldsymbol{v}_{pcc,2,abc}(s) \,.
\end{aligned}
\tag{6}
$$

The entries of the (transfer) matrices $\boldsymbol{M}(s)$ and $\boldsymbol{N}(s)$ in (6) are complex variables with magnitudes $M_{ij,n}$, $N_{ij,n}$ and angles $\gamma_{ij,n}$, $\varphi_{ij,n}$, respectively. By replacing s with $\jmath n\omega_g$ in $\boldsymbol{M}(s)$ and $\boldsymbol{N}(s)$, where ω_g is the grid angular frequency, the impact of the nth voltage harmonic (due to the different sources) on the nth PCC current harmonic can be found.

Similarly, the PCC voltage can also be computed in the frequency domain using the principle of superposition according to

$$
\begin{aligned}
\boldsymbol{v}_{pcc}(s) &= \boldsymbol{v}_{pcc,1}(s) + \boldsymbol{v}_{pcc,2}(s) \\
&= \boldsymbol{H}_2(s) \boldsymbol{u}_{abc}(s) + \boldsymbol{H}_4(s) \boldsymbol{v}_{pcc,2,abc}(s) \,.
\end{aligned}
\tag{7}
$$

Hence, as with (6), by using

$$
\boldsymbol{v}_{pcc,abc}(s) = \boldsymbol{M}'(s) \boldsymbol{u}_{abc}(s) + \boldsymbol{N}'(s) \boldsymbol{v}_{pcc,2,abc}(s) \,, \tag{8}
$$

and by replacing s with $\jmath n\omega_g$, the combined effect of different harmonic voltage sources to the PCC voltage can be found for each harmonic order ($n > 1$).

B. Conventional Two-Level OPPs

Consider the 2π-periodic switching signal $u(\theta)$ that exhibits quarter- and half-wave symmetry (QaHWS). Assuming a two-level converter, $u(\theta)$ is fully described by d switching angles $\alpha_i \in [0, \pi/2]$, $i \in \{1, \ldots, d\}$, and $d + 1$ switch positions $u_i \in \{-1, 1\}$, $i \in \{0, \ldots, d\}$, that occur in the first quarter of the fundamental period, while the initial switch position u_0 can

be either positive, i.e., $u_0 = 1$, or negative, i.e., $u_0 = -1$. Note that for a three-phase balanced system, it suffices to compute $u(\theta)$ offline for one phase, e.g., phase a, implying $u_a \equiv u(\theta)$, as u_b and u_c can be easily obtained by appropriately phase-shifting $u(\theta)$.

Given the above, the single-phase switching signal $u(\theta)$ can be described by the following Fourier series

$$u(\theta) = a_0 + \sum_{n=1}^{\infty} \left(a_n \cos(n\theta) + b_n \sin(n\theta) \right), \qquad (9)$$

with the Fourier coefficients

$$b_n = u_0 \frac{4}{n\pi} \left(1 + 2 \sum_{i=1}^{d} (-1)^i \cos(n\alpha_i) \right), \quad n = 1, 3, 5, \ldots . \tag{10}$$

Note that, due to the QaHWS, $u(\theta)$ consists only of odd harmonics, while all a_n Fourier coefficients are zero.

OPPs are typically computed such that they produce the lowest possible output current TDD, defined as

$$I_{\text{TDD}} = \frac{1}{\sqrt{2} I_{\text{nom}}} \sqrt{\sum_{n \neq 1} \hat{i}_{a,n}^2}, \tag{11}$$

with I_{nom} being the rms value of the nominal current, and $\hat{i}_{a,n}$ the amplitude of the nth PCC current harmonic in phase a. To this aim, the conventional OPP optimization problem for a grid-connected converter with an LCL filter is

$$\underset{\boldsymbol{\alpha}_Q = [\alpha_1 \ldots \alpha_d]^T}{\text{minimize}} \sum_{n=5,7,\ldots} \left(\frac{g_n}{n} \left(1 + 2 \sum_{i=1}^{d} (-1)^i \cos(n\alpha_i) \right) \right)^2 \tag{12a}$$

$$\text{subject to} \quad b_1 = m \tag{12b}$$

$$0 \leq \alpha_1 \leq \alpha_2 \leq \ldots \leq \alpha_d \leq \frac{\pi}{2} \tag{12c}$$

$$u_0 \in \{-1, 1\}, \tag{12d}$$

where $m \in [0, 4/\pi]$ is the modulation index, and g_n is the norm of the transfer matrix $\boldsymbol{H}_1(\jmath n\omega_g)$.[2] Moreover, constraint (12c) guarantees that the switching angles are in ascending order. Finally, note that (12a) does not consider triplen current harmonics ($n = 3, 9, \ldots$) as these are common-mode harmonics. Thus, these harmonics are zero in a three-phase balanced system, where it is assumed that the load is in a wye configuration and its star point is floating.

C. QaHWS OPPs That Account for Disturbances

Similar to (9), the a-phase disturbance voltage at the PCC can be represented with a Fourier series as

$$v_{\text{pcc},2,a}(\theta) = \sum_{n=1}^{\infty} \left(a_n' \cos(n\theta) + b_n' \sin(n\theta) \right). \tag{13}$$

---

[2]For more details on the derivation of (12), the reader is referred to [11].

To find the amplitude of the nth PCC current harmonic in phase a, (9) and (13) are used in combination with (6), yielding

$$\hat{i}_{\text{pcc},a,n} = \Big((a_n Q_{1,n} + b_n Q_{2,n} + a_n' Q_{3,n} + b_n' Q_{4,n})^2$$
$$+ (-a_n Q_{2,n} + b_n Q_{1,n} - a_n' Q_{4,n} + b_n' Q_{3,n})^2 \Big)^{1/2}, \tag{14}$$

where functions $Q_{i,n}$, $i = 1, \ldots, 4$, depend on the entries of matrices $\boldsymbol{M}(s)$ and $\boldsymbol{N}(s)$ for each harmonic order n, see (21) in the appendix.

In the sequel, for the sake of simplicity but without any loss of generality, it is assumed that the voltage disturbance at the PCC has QaHWS, i.e., $a_n' = 0$, and the amplitudes of its harmonics are equal to the maximum levels allowed by the grid standard IEC 61000-2-4 [2], i.e., $b_n' = \hat{v}_{n,\max}$. Given this, and by considering that the disturbance harmonics affect the current harmonics at the PCC, the current TDD produced by QaHWS OPPs becomes

$$I_{\text{TDD}} = \underbrace{\frac{1}{\sqrt{2} I_{\text{nom}}}}_{c} \Bigg(\sum_{n=5,7,\ldots} \Big((b_n Q_{2,n} + \hat{v}_{n,\max} Q_{4,n})^2$$
$$+ (b_n Q_{1,n} + \hat{v}_{n,\max} Q_{3,n})^2 \Big) \Bigg)^{1/2}, \tag{15}$$

where (11) and (14) are used. The current TDD in (15) can be written as $I_{\text{TDD}} = c \sqrt{J_{\text{QaHWS}}}$, where c depends only on the nominal current, and it is thus constant. This means c can be discarded, leaving J_{QaHWS} to serve as the objective function. Hence, the optimization problem for QaHWS OPPs that produce minimum PCC current TDD, while accounting for the LCL filter and harmonic disturbances at the PCC is

$$\underset{\boldsymbol{\alpha}_Q}{\text{minimize}} \quad J_{\text{QaHWS}} \tag{16a}$$

$$\text{subject to} \quad b_1 = m \tag{16b}$$

$$0 \leq \alpha_1 \leq \alpha_2 \leq \ldots \leq \alpha_d \leq \frac{\pi}{2} \tag{16c}$$

$$u_0 \in \{-1, 1\}. \tag{16d}$$

D. Constrained HWS OPPs That Account for Disturbances

As shown in [12], relaxing the symmetry of the OPP from QaHWS to half-wave symmetry (HWS) increases the degrees of freedom in the optimization problem, thus allowing for further improvement of the current TDD. In doing so, however, the number of the to-be-computed switching angles increases from d to $2d + 1$, i.e., $\alpha_i \in [0, \pi]$, $i \in \{1, \ldots, 2d + 1\}$ [17]. Moreover, HWS implies that the Fourier coefficients of the single-phase OPP in (9) are non-zero for odd harmonics, and are given by

$$a_n = -u_0 \frac{4}{n\pi} \sum_{i=1}^{2d+1} (-1)^i \sin(n\alpha_i), \quad n = 1, 3, 5, \ldots$$

$$b_n = +u_0 \frac{4}{n\pi} \sum_{i=1}^{2d+1} (-1)^i \cos(n\alpha_i), \quad n = 1, 3, 5, \ldots . \tag{17}$$

As a result, the current TDD for HWS OPPs is given by

$$I_{\text{TDD}} = \underbrace{\frac{1}{\sqrt{2}I_{\text{nom}}}}_{c} \left(\sum_{n=5,7,\dots} \left(u_0 \frac{-4Q_{1,n}}{n\pi} \sum_{i=1}^{2d+1} (-1)^i \sin(n\alpha_i) \right. \right.$$

$$\left. + u_0 \frac{4Q_{2,n}}{n\pi} \sum_{i=1}^{2d+1} (-1)^i \cos(n\alpha_i) + \hat{v}_{n,\max} Q_{4,n} \right)^2$$

$$+ \left(u_0 \frac{4Q_{2,n}}{n\pi} \sum_{i=1}^{2d+1} (-1)^i \sin(n\alpha_i) \right.$$

$$\left. \left. + u_0 \frac{4Q_{1,n}}{n\pi} \sum_{i=1}^{2d+1} (-1)^i \cos(n\alpha_i) + \hat{v}_{n,\max} Q_{3,n} \right)^2 \right)^{1/2},$$

$$(18)$$

which is of the form $I_{\text{TDD}} = c\sqrt{J_{\text{HWS}}}$.

The goal of the proposed OPPs is—besides producing an output current with as low a TDD as possible—to guarantee that individual current and voltage harmonics do not exceed the limits imposed by the harmonic grid standards, even in the presence of harmonic disturbances at the PCC. To this end, *harmonic-constrained* HWS OPPs are computed by adding explicit constraints to the OPP optimization problem. Specifically, the relevant problem is of the form

$$\underset{\boldsymbol{\alpha}_H, \boldsymbol{\epsilon}}{\text{minimize}} \quad J_{\text{HWS}} + \boldsymbol{\epsilon}^T \boldsymbol{W} \boldsymbol{\epsilon} \tag{19a}$$

$$\text{subject to} \quad b_1 = m \tag{19b}$$

$$a_1 = 0 \tag{19c}$$

$$0 \leq \alpha_1 \leq \alpha_2 \leq \dots \leq \alpha_{2d+1} \leq \pi \tag{19d}$$

$$\hat{i}_{\text{pcc},a,n} \leq \hat{i}_{n,\max} + \epsilon_{i,n}, \quad n \in \mathbb{N}_1 \tag{19e}$$

$$\hat{v}_{\text{pcc},a,n} \leq \hat{v}_{n,\max} + \epsilon_{v,n}, \quad n \in \mathbb{N}_1 \tag{19f}$$

$$\hat{u}_n \leq \min\left(\frac{\hat{v}_{n,\max}}{g'_n}, \frac{\hat{i}_{n,\max}}{g_n} \right) + \epsilon_{u,n}, \ n \in \mathbb{N}_2 \tag{19g}$$

$$\epsilon_{i,n} \geq 0, \ \epsilon_{v,n} \geq 0, \ \epsilon_{u,n} \geq 0 \tag{19h}$$

$$u_0 \in \{1, -1\}, \tag{19i}$$

where the switching angles $\boldsymbol{\alpha}_H = [\alpha_1 \ \dots \ \alpha_{2d+1}]^T$ constitute the optimization variables. Moreover, constraints (19b) and (19c) ensure that the amplitude of the fundamental OPP component is equal to the desired modulation index m, while its phase is zero.

Focusing on the harmonic constraints, as can be observed from (19), there are constraints on the amplitude of both current and voltage harmonics. The amplitude of the current harmonics in (19e) is given by (14). As for the voltage harmonic constraints in (19f), the amplitude of the nth a-phase voltage harmonic at the PCC can be found with the help of (8), (9), and (13), according to

$$\hat{v}_{\text{pcc},a,n} = \left((a_n Q_{5,n} + b_n Q_{6,n} + a'_n Q_{7,n} + b'_n Q_{8,n})^2 \right.$$

$$\left. + (-a_n Q_{6,n} + b_n Q_{5,n} - a'_n Q_{8,n} + b'_n Q_{7,n})^2 \right)^{1/2}, \tag{20}$$

TABLE I: Rated values of the system

Parameter	Symbol	SI Value
Voltage	V_R	400 V
Current	I_R	18 A
Angular grid frequency	ω_{gR}	$2\pi 50$ rad/s
Short-circuit ratio	k_{sc}	13.4
Grid impedance ratio	k_{XR}	7

TABLE II: System parameters

Grid	Inductance	L_g	3 mH
	Resistance	R_g	136 mΩ
Other	Inductance	L_d	6 mH
converters	Resistance	R_d	269 mΩ
LCL filter	Converter-side inductance	L_{fc}	6.6 mH
	Converter-side resistance	R_{fc}	100 mΩ
	Capacitance	C	8.8 μF
	Capacitor resistance	R_c	0.8 mΩ
	Grid-side inductance	L_{fg}	6 mH
	Grid-side resistance	R_{fg}	70 mΩ
Converter	Dc-link	V_{dc}	650 V

with $Q_{i,n}$, $i = 5, \dots, 8$, being functions of the entries of matrices $\boldsymbol{M}'(s)$ and $\boldsymbol{N}'(s)$ for each harmonic order, see (22) in the appendix.

The goal of both (19e) and (19f) is to limit the current and voltage harmonics, respectively, at the PCC to the levels allowed by the grid standards. These constraints are imposed only on the harmonics in $\mathbb{N}_1$, i.e., harmonics for which the voltage disturbance has non-zero harmonics. On the other hand, constraint (19g) is imposed on the harmonics in $\mathbb{N}_2$ for which the voltage disturbance does not have harmonics. This constraint maps the limits on the amplitude of the nth PCC current and voltage harmonics, as dictated respectively by the standards [1] and [2], to the amplitude of the switching signal harmonic—i.e., $\hat{u}_n = \sqrt{a_n^2 + b_n^2}$—via the gains g_n and g'_n. These gains are the norms of the transfer matrices $\boldsymbol{H}_1(\jmath n\omega_g)$ and $\boldsymbol{H}_2(\jmath n\omega_g)$ respectively, see Section II-A.

Finally, it is important to mention that problem (19) imposes soft constraints on the individual harmonics to avoid feasibility issues associated with hard constraints. To nevertheless minimize potential constraint violations, the slack variables $\epsilon_{i,n}$, $\epsilon_{v,n}$, and $\epsilon_{u,n}$—aggregated into the vector $\boldsymbol{\epsilon} = [\boldsymbol{\epsilon}_i^T \ \boldsymbol{\epsilon}_v^T \ \boldsymbol{\epsilon}_u^T]^T$, where $\boldsymbol{\epsilon}_i$ and $\boldsymbol{\epsilon}_v$ comprise the slack variables $\epsilon_{i,n}$ and $\epsilon_{v,n}$, respectively, for $n \in \mathbb{N}_1$, and $\boldsymbol{\epsilon}_u$ consists of $\epsilon_{u,n}$ for $n \in \mathbb{N}_2$—are introduced along with the (diagonal) weighting matrix $\boldsymbol{W}$. The non-zero entries of the latter are chosen such that the violation of the soft constraints is heavily penalized. As a result, $\boldsymbol{\epsilon}$ is also an optimization variable.

III. NUMERICAL RESULTS

This section assesses the performance of the proposed OPPs. To allow for meaningful conclusions, five different modulation
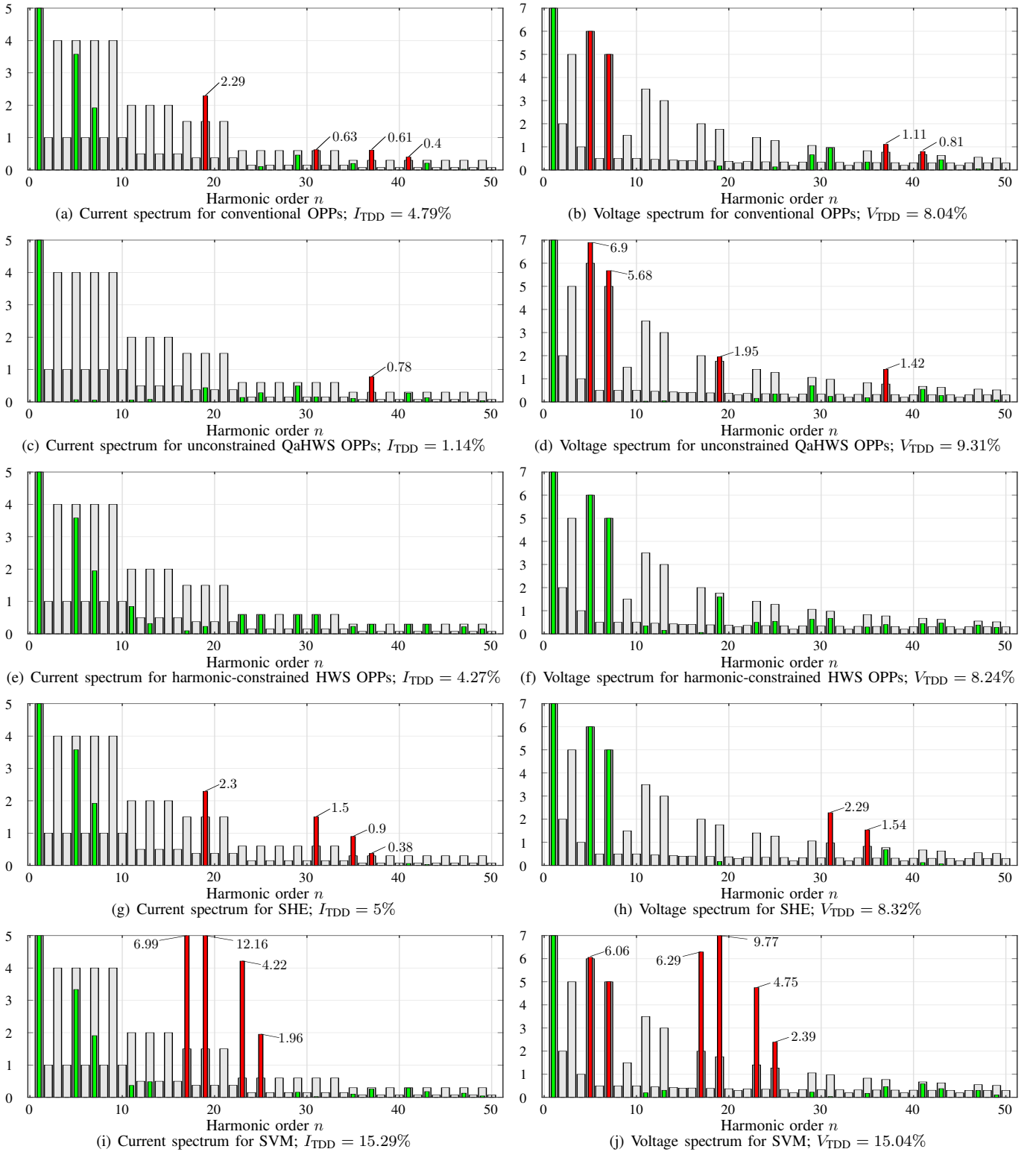
Fig. 3: Current and voltage harmonics at the PCC (%) for $m = 1.0785$. The grid standard limits are shown as light gray bars, harmonics that meet them are shown as green bars, while harmonics that violate them are shown as red bars. A switching frequency of 1050 Hz is considered.

methods are compared, namely (a) conventional OPPs, i.e., OPPs obtained with (12), (b) unconstrained QaHWS OPPs computed with (16), (c) the proposed harmonic-constrained HWS OPPs computed with (19), (d) SHE, and (e) SVM.

All the above-mentioned modulation schemes are used with a grid-connected two-level converter with an LCL filter. The rated values of the system under consideration are presented in Table I. The converter has $12.5\,\text{kVA}$ rated power and a dc-link

voltage of 650 V, see Table II. The filter resonance frequency is $f_{\text{res}} = 957$ Hz, as can be deduced from its parameters provided in Table II.

To showcase how each modulation method behaves in the presence of harmonic disturbances at the PCC, it is assumed that other grid customers inject a 5th and a 7th voltage harmonic to the PCC with amplitudes equal to the maximum levels allowed by the IEC 61000-2-4 standard. In addition, to provide more insight, a 19th harmonic is also considered, i.e., close to the filter resonance frequency f_{res}, with an amplitude of $0.1\hat{v}_{19,\max}$. Finally, regarding the chosen operating conditions, operation at modulation index $m = 1.0785$ is chosen since grid-connected converters are typically operated between $m = 1$ and 1.1. Moreover, for a fair comparison, all modulation schemes achieve a switching frequency of $f_{\text{sw}} = 1050$ Hz, implying that OPPs with $d = 10$ are used.

The current and voltage harmonic spectra resulted from the aforementioned modulation schemes are illustrated in Fig. 3. More specifically, the harmonic spectra of the PCC current and voltage for conventional OPPs are depicted in Figs. 3(a) and 3(b), respectively. Comparing the amplitude of individual harmonics with their permissible levels, it is observed that several current and voltage harmonics violate their limits. Notably, as can be seen in Fig. 3(a), the 19th disturbance voltage harmonic injected into the PCC gives rise to a current harmonic of the same order that has considerably higher amplitude than its limit.

The harmonic spectra for the unconstrained QaHWS OPPs—see Figs. 3(c) and 3(d)—reveal that, when voltage disturbances are considered in the OPP optimization problem, the current TDD, i.e., the sole objective of problem (16), is effectively minimized, resulting in a very low current TDD of $I_{\text{TDD}} = 1.14\%$. Nevertheless, as these OPPs do not try to actively mitigate the injected PCC voltage harmonics, individual harmonics violate their limits. This is particularly the case with voltage harmonics as the harmonics injected by the converter are amplified by those injected by other converters, leading to significant violations in the harmonic voltage standards, and a high voltage TDD.

To address the above, and thus ensure that all current and voltage harmonics comply with the grid standards even in the presence of harmonic disturbances at the PCC, the proposed harmonic-constrained HWS OPPs are computed based on (19) while imposing constraints on the first 18 non-triplen odd harmonics. The resulting current and voltage harmonic spectra demonstrate that all harmonics are within their permissible range, see Figs. 3(e) and 3(f). Naturally, as the OPP harmonics are manipulated so that the standards are met, the converter injects such harmonics that slightly compromise the overall current quality at the PCC, thus increasing its TDD value to 4.27%. Nevertheless, this value is still lower than the 5% required by the grid codes, while the voltage quality has been improved. Hence, as can be seen, the proposed OPPs ensure that the harmonic grid standards are fully met for *both* the voltage and current. This demonstrates that, thanks to the

proposed formulation of the OPP problem (19), the computed OPPs fulfill the intended goals, ensuring favorable harmonic performance.

Following, the harmonic spectra obtained with SHE that eliminates all non-triplen odd harmonics in the range $n \in [5, 29]$ are shown in Figs. 3(g) and 3(h). As can be seen, the presence of the disturbance harmonics does not allow the 19th harmonic to be zero, as was expected it to be due to the targeted elimination. Moreover, some of the harmonics of order greater than $n > 29$ exceed their limits, while both I_{TDD} and V_{TDD} are higher than those of the proposed OPPs.

Finally, the comparisons are concluded with the SVM method implemented by means of asymmetric regularly sampled CB-PWM with min/max common-mode voltage injection [3]. Comparing the harmonic spectra produced by the proposed harmonic-constrained OPPs with those of SVM (Figs. 3(i) and 3(j)), it is clear that the harmonic amplitudes of the latter are significant, as verified by 15.29% and 15.04% current and voltage TDDs, respectively. As a result, individual voltage and current harmonics significantly exceed their limits, indicating that SVM is not suitable for the specific application.

IV. Conclusions

This paper presented the computation of OPPs for grid-connected converters with LCL filters while taking harmonic disturbances at the PCC into account. To fully respect the harmonic grid codes in the presence of disturbances, a suitable harmonic mathematical model is first derived. Subsequently, the OPP optimization problem is formulated such that the objective function accounts for the harmonic disturbances, while explicit constraints on current and voltage harmonics ensure that individual harmonics do not violate their stringent limits. Moreover, the assumption of QaHWS on the switching signal is dropped to allow for the manipulation of both the amplitude and phase of harmonics, thus equipping the optimizer with more degrees of freedom. Thanks to the above, as demonstrated by the presented numerical results, the proposed harmonic-constrained HWS OPPs not only outperform conventional modulation methods, such as SVM, but achieve a better harmonic performance than that of SHE and conventional OPPs.

Even though the presented approach can provide OPPs that effectively shape their harmonic spectrum to account for injected PCC voltage harmonics, it comes with some limitations. Specifically, the assumption of known harmonic disturbances—in terms of order, phase, and amplitude—limits the applicability of the computed OPPs. Since the offline optimization procedure is based on a model built around this assumption, the harmonic performance of the computed OPPs may deteriorate in the presence of harmonics with different characteristics. However, computing OPPs for different harmonics would result in extensive look-up-tables, rendering this option impractical. Therefore, a more suitable option could be to either compute OPPs that are robust to variations in harmonics [18], or derive them in real time.

APPENDIX

Functions $Q_{i,n}$, $i = 1, \ldots, 4$, that form the amplitude of the nth a-phase PCC current harmonic in (14) are

$$
\begin{aligned}
Q_{1,n} = {} & M_{11,n} \cos(\gamma_{11,n}) + M_{12,n} \cos\left(\gamma_{12,n} - n\frac{2\pi}{3}\right) \\
& + M_{13,n} \cos\left(\gamma_{13,n} - n\frac{4\pi}{3}\right), \\
Q_{2,n} = {} & M_{11,n} \sin(\gamma_{11,n}) + M_{12,n} \sin\left(\gamma_{12,n} - n\frac{2\pi}{3}\right) \\
& + M_{13,n} \sin\left(\gamma_{13,n} - n\frac{4\pi}{3}\right), \\
Q_{3,n} = {} & N_{11,n} \cos(\varphi_{11,n}) + N_{12,n} \cos\left(\varphi_{12,n} - n\frac{2\pi}{3}\right) \\
& + N_{13,n} \cos\left(\varphi_{13,n} - n\frac{4\pi}{3}\right), \\
Q_{4,n} = {} & N_{11,n} \sin(\varphi_{11,n}) + N_{12,n} \sin\left(\varphi_{12,n} - n\frac{2\pi}{3}\right) \\
& + N_{13,n} \sin\left(\varphi_{13,n} - n\frac{4\pi}{3}\right).
\end{aligned}
\tag{21}
$$

Similarly, functions $Q_{i,n}$, $i = 5, \ldots, 8$, making up the amplitude of the nth a-phase PCC voltage harmonic in (20), are given by

$$
\begin{aligned}
Q_{5,n} = {} & M'_{11,n} \cos(\gamma'_{11,n}) + M'_{12,n} \cos\left(\gamma'_{12,n} - n\frac{2\pi}{3}\right) \\
& + M'_{13,n} \cos\left(\gamma'_{13,n} - n\frac{4\pi}{3}\right), \\
Q_{6,n} = {} & M'_{11,n} \sin(\gamma'_{11,n}) + M'_{12,n} \sin\left(\gamma'_{12,n} - n\frac{2\pi}{3}\right) \\
& + M'_{13,n} \sin\left(\gamma'_{13,n} - n\frac{4\pi}{3}\right), \\
Q_{7,n} = {} & N'_{11,n} \cos(\varphi'_{11,n}) + N'_{12,n} \cos\left(\varphi'_{12,n} - n\frac{2\pi}{3}\right) \\
& + N'_{13,n} \cos\left(\varphi'_{13,n} - n\frac{4\pi}{3}\right), \\
Q_{8,n} = {} & N'_{11,n} \sin(\varphi'_{11,n}) + N'_{12,n} \sin\left(\varphi'_{12,n} - n\frac{2\pi}{3}\right) \\
& + N'_{13,n} \sin\left(\varphi'_{13,n} - n\frac{4\pi}{3}\right).
\end{aligned}
\tag{22}
$$

REFERENCES

[1] IEEE Std 519-2014 (Revision of IEEE Std 519-1992), "IEEE recommended practices and requirements for harmonic control in electrical power systems," pp. 1–29, Jun. 2014.

[2] IEC Std 61000-2-4, "Electromagnetic compatibility (EMC)—part 2-4: Environment—compatibility levels in industrial plants for low-frequency conducted disturbances," Sep. 2002.

[3] D. G. Holmes and T. A. Lipo, *Pulse width modulation for power converters: Principles and practice.* Piscataway, NJ, USA: IEEE Press, 2003.

[4] H. S. Patel and R. G. Hoft, "Generalized techniques of harmonic elimination and voltage control in thyristor inverters: Part I—Harmonic elimination," *IEEE Trans. Ind. Appl.*, vol. IA-9, no. 3, pp. 310–317, May/Jun. 1973.

[5] G. S. Buja, "Optimum output waveforms in PWM inverters," *IEEE Trans. Ind. Appl.*, vol. IA-16, no. 6, pp. 830–836, Nov./Dec. 1980.

[6] J. Pontt, J. Rodriguez, and R. Huerta, "Mitigation of noneliminated harmonics of SHEPWM three-level multipulse three-phase active front end converters with low switching frequency for meeting standard IEEE-519-92," *IEEE Trans. Power Electron.*, vol. 19, no. 6, pp. 1594–1600, Nov. 2004.

[7] L. G. Franquelo, J. Nápoles, R. C. P. Guisado, J. I. León, and M. A. Aguirre, "A flexible selective harmonic mitigation technique to meet grid codes in three-level PWM converters," *IEEE Trans. Ind. Electron.*, vol. 54, no. 6, pp. 3022–3029, Dec. 2007.

[8] J. Nápoles, A. J. Watson, J. J. Padilla, J. I. León, L. G. Franquelo, P. W. Wheeler, and M. A. Aguirre, "Selective harmonic mitigation technique for cascaded H-bridge converters with nonequal dc link voltages," *IEEE Trans. Ind. Electron.*, vol. 60, no. 5, pp. 1963–1971, May 2013.

[9] A. Moeini, H. Iman-Eini, and M. Bakhshizadeh, "Selective harmonic mitigation–pulse-width modulation technique with variable dc-link voltages in single and three-phase cascaded H-bridge inverters," *IET Power Electron.*, vol. 7, no. 4, pp. 924–932, Apr. 2014.

[10] T. Dorfling, H. d. T. Mouton, and T. Geyer, "Generalized model predictive pulse pattern control based on small-signal modeling—Part 2: Implementation and analysis," *IEEE Trans. Power Electron.*, vol. 37, no. 9, pp. 10488–10498, Sep. 2022.

[11] S. Rahmanpour, P. Karamanakos, and T. Geyer, "Three-level optimized pulse patterns for grid-connected converters with LCL filters," in *Proc. IEEE Energy Convers. Congr. Expo.*, Nashville, TN, USA, Oct. 2023, pp. 1430–1437.

[12] A. Birth, T. Geyer, H. d. T. Mouton, and M. Dorfling, "Generalized three-level optimal pulse patterns with lower harmonic distortion," *IEEE Trans. Power Electron.*, vol. 35, no. 6, pp. 5741–5752, Jun. 2020.

[13] T. Geyer, P. Karamanakos, and I. Koukoula, "Optimized pulse patterns with bounded semiconductor losses," *IEEE Trans. Power Electron.*, vol. 39, no. 3, pp. 3233–3243, Mar. 2024.

[14] I. Koukoula, P. Karamanakos, and T. Geyer, "Optimal pulse width modulation of three-level converters with reduced common-mode voltage," *IEEE Trans. Ind. Appl.*, vol. 60, no. 3, pp. 4062–4075, May/Jun. 2024.

[15] A. Moeini, H. Zhao, and S. Wang, "A current-reference-based selective harmonic current mitigation PWM technique to improve the performance of cascaded H-bridge multilevel active rectifiers," *IEEE Trans. Ind. Electron.*, vol. 65, no. 1, pp. 727–737, Jan. 2018.

[16] I. Ibanez-Hidalgo, A. Sanchez-Ruiz, A. Perez-Basante, A. Zubizarreta, S. Ceballos, S. Gil-Lopez, and R. P. Aguilera, "Real time selective harmonic control—PWM based on artificial neural networks," *IEEE Trans. Power Electron.*, vol. 39, no. 1, pp. 768–783, Jan. 2024.

[17] E. Kontodinas, P. Karamanakos, A. Kraemer, and S. Wendel, "Optimized pulse patterns for anisotropic synchronous machines with improved current and torque properties," in *Proc. Eur. Conf. on Power Electron. and Applicat.*, Aalborg, Denmark, Sep. 2023, pp. 1–8.

[18] O. Karaca and I. Tsoumas, "Robust optimized pulse patterns for salient permanent magnet synchronous machines," in *Proc. Eur. Conf. on Power Electron. and Applicat.*, Aalborg, Denmark, Sep. 2023, pp. P.1–P.9.